Journal of Computers Vol. 34 No. 3, June 2023, pp. 165-178
doi: 10.53106/199115992023063403012

Research on Influence of Distributed Energy Accessing Power Grid System Based on Integral Projection Algorithm

Yonggang Dong*, Shichao Cao, Haoliang Yang

Hebei Vocational University of Technology and Engineering, Xingtai City, Hebei 054002, China

ygdong2022@163.com

Received 29 June 2022; Revised 4 October 2022; Accepted 12 December 2022

Abstract. A large number of distributed energy sources connected to the grid will cause certain disturbances to the stability of the grid system. We consider the random characteristics and establish a dynamic simulation framework for the active power distribution system suitable for the integral projection algorithm. The article uses an internal integrator to solve the fast dynamic process with explicit and implicit Euler methods in small steps. In the calculation process, this method can effectively consider the influence of events such as fault disturbance on the grid connection of the distributed power grid. Numerical analysis and simulation tests verify the effectiveness of this algorithm.

Keywords: distributed energy, power grid system, implicit projection integral algorithm, differential-algebraic equation, distributed energy

1 Introduction

The connection of a large number of distributed energy sources to the power distribution system will significantly change the structure and operation of the power system at medium and low voltage levels. The access to distributed power makes the power distribution system develop from the traditional radial network structure to the multi-source grid structure. Distributed energy has rich meanings. It includes distributed power generation equipment such as photovoltaics and wind turbines and generalized controllable energy sources such as distributed energy storage, controllable loads, and electric vehicles. Smart grids take the opportunity of widespread access to distributed energy sources to achieve adequate control of small-scale systems in local areas. Access to distributed energy can optimize advanced new power distribution technologies such as microgrids, virtual power plants, unit control areas, and AC/DC hybrid power distribution.

The stability simulation after the distributed energy is connected to the power grid focuses on analyzing the dynamic response characteristics of the power frequency electrical quantities under the system disturbance during the operation of the power grid. System disturbance simulation can be used in many aspects, such as controller design and control strategy verification of microgrids, fault characteristic analysis, etc. Power grid stability simulation is an extension of the traditional power system transient stability simulation work at the low-voltage distribution level. Still, it also faces many challenges, such as model diversity, system rigidity, and simulation rapidity.

In response to the above problems, researchers have done much research. Taking the stability problem caused by the access to distributed power sources with a high penetration rate as an example, Min, W. et al. proposed the concept of "virtual inertia." The synchronous virtual machine (VSG) technology is the most typical [1]. The synchronous virtual machine offers a new power electronic control strategy for controllable distributed power generation. This method makes the distributed power supply simulate the traditional synchronous generator during operation. The dynamic behavior then provides virtual rotor rotational inertia to the power grid. This can make up for the lack of inertia caused by access to many powerful electronic devices. In addition, the dynamic characteristics and control strategies of independent, active power distribution systems are studied, and intelligent soft switching [2-3] and other related academic research have become a research hotspot in the field of dynamic power distribution systems recently.

The dynamic simulation of an active power distribution system has the characteristics of multiple time scales. It is reflected mathematically as a severe problem. There has been a lot of theoretical and methodological research on solving the multi-time-scale problem in the traditional power system transient stability simulation.

* Corresponding Author

Singh, J., & Tiwari, R. introduced a numerical integration method based on system matrix index into power system brief stability simulation analysis [4]. The process can obtain accurate solutions to linear problems and has good numerical stability. The numerical integration method based on the system matrix index can adopt a larger simulation step size to improve the simulation calculation efficiency. However, the solution of this method is complicated. Compared with the classical way, it has poor generality, and the implementation of the algorithm is complex. Zhen, T et al. proposed a variable-step numerical integration method to solve this problem [5]. The simulation step size can be adaptively adjusted according to the time constant of the dynamic characteristics of the power system. Most of this literature adopts the implicit numerical integration method to take advantage of its good numerical stability. However, the implicit process is complicated to solve per time step. Its solution efficiency is low when a small step size simulation is performed.

The dynamic operating characteristics of active power distribution systems are complex. It may require a long-time small step simulation to analyze its fast dynamic response characteristics. Simply using the implicit integration method can seriously affect the simulation time. To this end, Butt, O. M. et al. proposed a decoupling simulation method [6]. Firstly, the simulation system is divided into a rigid subsystem with smaller dimensions and a non-rigid subsystem according to the time constant of its dynamic running characteristics. They used the direct integration method to solve the non-rigid subsystem to improve the efficiency of simulation calculation and used the implicit method to solve the rigid subsystem to ensure the numerical stability of the process. However, the dimension of the wooden part of this method is significantly increased for the active power distribution system with high permeability distributed power generation. This makes the decoupling method no longer significantly improve the computational efficiency. In addition, this method needs to consider the synchronization problem of the simulation step size of the explicit and implicit integration methods, which makes the variable step size method challenging to apply to the decoupling simulation method directly.

Because of this, this paper proposes a dynamic simulation method of an active power distribution system based on an implicit projection integration algorithm. The process considers the stochastic dynamic operating characteristics of the simulation of active power distribution systems. The main work and innovations of this paper are summarized as follows:

1) In this paper, a dynamic simulation architecture of an active power distribution system that considers random characteristics and is suitable for projection integration algorithms is constructed. The architecture builds differential-algebraic equations and stochastic differential-algebraic equations. It covers typical component models of active power distribution systems considering random disturbances. The system can accurately simulate the multi-time scale and random characteristics during the operation of the active power distribution system. At the same time, the architecture can be solved by numerical algorithms of ordinary differential equations and stochastic differential equations. 2) Aiming at the rigidity problem in the dynamic simulation of active power distribution systems, this paper proposes a projection integration algorithm suitable for multi-time-scale dynamic simulation of the active power distribution systems. This paper uses different scales of active power distribution system test examples based on different simulation scenarios to test the algorithm. The system verifies the accuracy and efficiency of the projection integration algorithm. Finally, this paper takes the virtual synchronous machine access as an example to analyze the influence of the new control strategy on the dynamic operating characteristics of the active power distribution system.

2 Active Power Distribution System Modeling

The dynamic simulation mathematical model of the active power distribution system includes two parts: the differential equation describing the dynamic characteristics of the components and the algebraic equation describing the electrical connections between the components. The electrical relationship between the features may change during the system's operation. The content includes events or functions such as load switching, unit start and stop, and line breaking. If the relay protection device is considered, it also contains many continuous and (or) discrete logic time-varying parameters. We describe the mathematical model of the active power distribution system with a high-dimensional nonlinear differential-algebraic equation system:

$$\begin{cases} x = f(x, y, u, t) \\ 0 = g(x, y, u, t) \end{cases}. \tag{1}$$

$x(x \in R^{nx})$ is the system state variable. It represents motor rotor speed, power electronic device control, and load dynamic parameters. $y(y \in R^{ny})$ is an algebraic variable. It represents the bus voltage amplitude and phase angle. $u(u \in R^{nu})$ is a discrete variable. It means an event or operation. $t \in R^{+}$ is the time. An if-then statement can replace the discrete variable in formula (1).

$f\,(f: R^{nx} \times R^{ny} \mapsto R^{nx})$ is the differential equation. $g\,(g: R^{nx} \times R^{ny} \mapsto R^{ny})$ is an algebraic equation. The article describes the quasi-steady-state modeling method of PWM inverters. Then we introduced the dynamic simulation model of the typical DG of the active power distribution system.

2.1 The Quasi-steady-state Model of the PWM Converter

We do not consider the dynamic switching behavior of the power electronic converter circuit in the dynamic simulation analysis of the active power distribution system. The article only considers the circuit's fundamental frequency model and the dynamic characteristics of the controller link. We call it a quasi-steady-state modeling method for power electronic devices.

The article takes the model description of the network side in the synchronous coordinate system as a case. The quasi-steady-state model corresponding to the converter is shown in Fig. 1. $\dot{U}_1$ is the phasor of the converter output voltage (that is, the modulated voltage). $R_f + jX_f$ is the filter circuit parameter of LC at the outlet of the modulated voltage of the converter. $\dot{U}$ is the bus voltage phasor at the grid-connected point. $\dot{I}$ is the current output to the network side. It is represented by I_d, I_q in the $dq0$ coordinate system. It is represented by I_x, I_y in the $xy0$ coordinate system. PWM vector modulation can be described by equation (2).

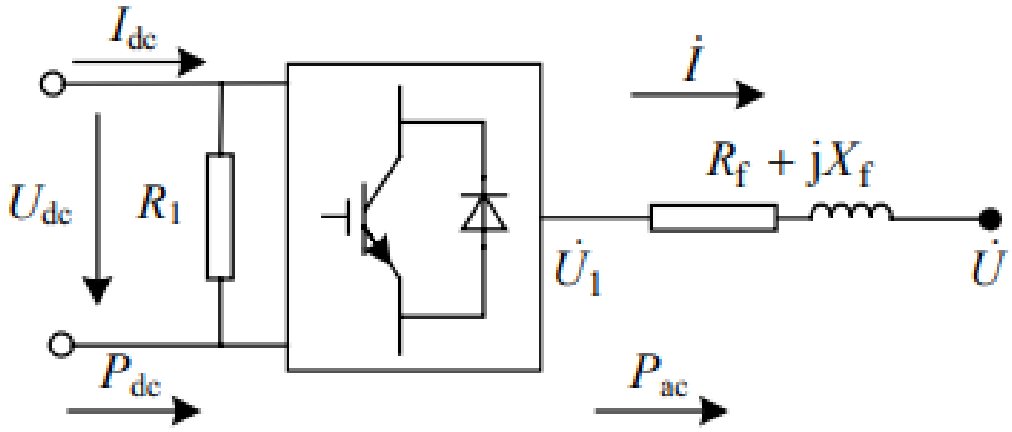

Fig. 1. Quasi-steady state model of PWM inverter circuit

$$\begin{cases} U_{1d} = \dfrac{K_0 P_{md} U_{dc}}{U_{acBASE}} \\ U_{1q} = \dfrac{K_0 P_{mq} U_{dc}}{U_{acBASE}} \end{cases}. \tag{2}$$

P_{md} and P_{mq} are the $dq0$ vector decoupling control components of the pulse width modulation coefficient of the converter. K_0 is the modulation factor. U_{dc} represents the famous value of DC side voltage. The voltage balance equation and active power equation of the feeder at the outlet of the converter are respectively expressed as follows

$$\begin{cases} U_{1q} = U_q + R_f I_q + X_f I_d \\ U_{1d} = U_d + R_f I_d - X_f I_q \end{cases}. \tag{3}$$

$$P_{ac} = U_x I_x + U_y I_y + (I_x^2 + I_y^2) R_f . \tag{4}$$

If we need to consider the converter loss, the relationship between the active power output on the AC side of the converter and the active power input on the DC side is expressed as follows.

$$P_{dc} = U_{dc} I_{dc} = P_{loss} + P_{ac} = \frac{U_{dc}^2}{R_1} + P_{ac}. \tag{5}$$

Equations (2)-(5) combined with the converter control link can form a quasi-steady-state model of the PWM converter.

2.2 Dynamic Modeling of a Photovoltaic Power Generation System

The photovoltaic grid-connected power generation system comprises photovoltaic arrays, power electronic conversion devices, maximum power controllers, and grid-connected controllers. Its single diode equivalent circuit model is shown in Fig. 2.

$$I = N_p I_{ph} - N_P I_S [e^{\frac{q}{AKT}(\frac{U}{N_S} + \frac{IR_S}{N_P})} - 1] - \frac{N_P}{R_{sh}}(\frac{U}{N_S} + \frac{IR_S}{N_P}). \tag{6}$$

U is the output voltage of the photovoltaic cell. I is the output current of the photovoltaic cell. I_{ph} is the saturation current of the diode diffusion effect. I_S is the diode saturation current. q is the electric electron quantity constant ($1.602 \times 10^{-19} C$). k is Boltzmann's constant ($1.381 \times 10^{-23} J / K$). T is the absolute temperature value of the photovoltaic cell. A is the fitting coefficient of diode characteristics.

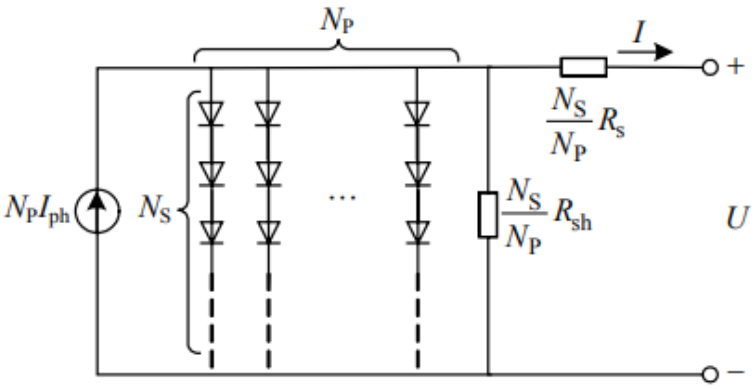

Fig. 2. Single diode model photovoltaic array equivalent circuit

The photovoltaic grid-connected power generation system adopts a standard single-stage grid-connected system. We directly use the inverter to convert the DC power output by the photovoltaic array into AC power to achieve grid connection (Fig. 3). This paper uses the disturbance observation method as the photovoltaic maximum power point tracking algorithm. The algorithm flow is shown in Fig. 4.

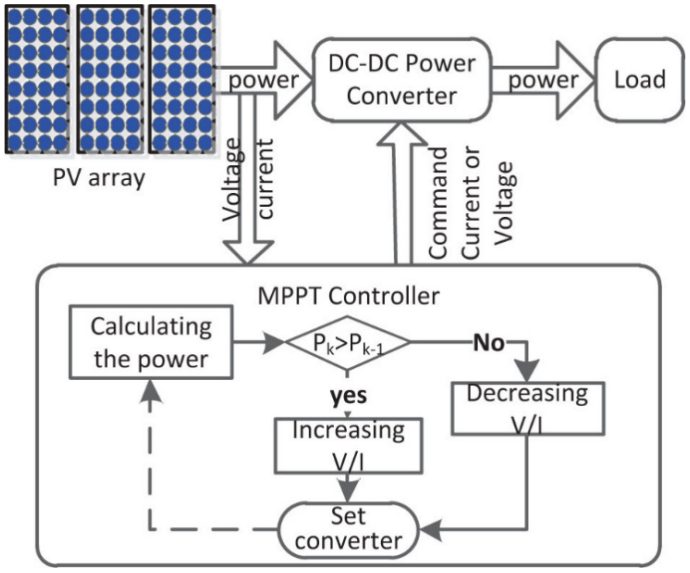

Fig. 3. Topological structure of single-stage photovoltaic grid-connected power generation system

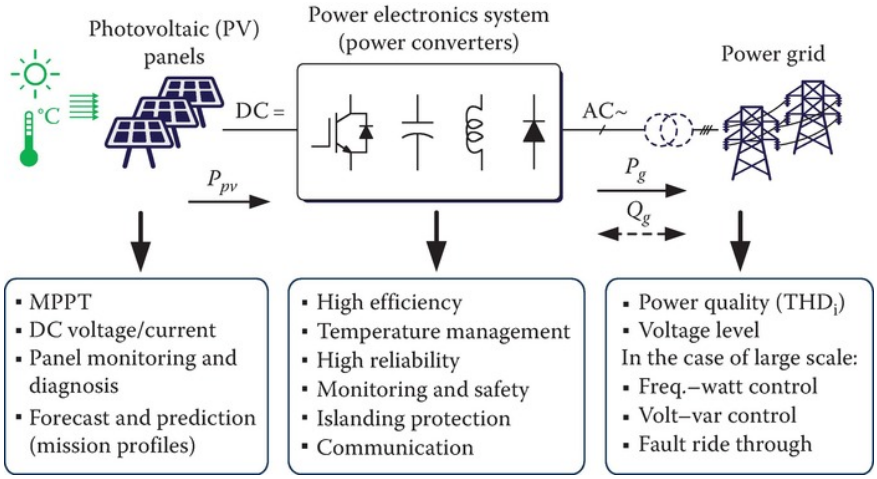

Fig. 4. Flow chart of the disturbance observation algorithm

2.3 Dynamic Modeling of Battery Energy Storage System

The battery grid-connected energy storage system comprises batteries, power electronic conversion devices, and grid-connected controllers. Among them, the battery often adopts a general model. The equivalent circuit is shown in Fig. 5. The available model of the battery is composed of the internal resistance R and the controlled voltage source E in series. Assuming that R remains unchanged during battery operation, E can be calculated by the formula (8).

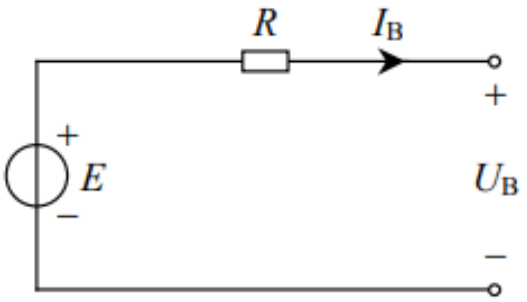

Fig. 5. Equivalent circuit of battery general model

$$E = E_0 - K\frac{C_{\max}}{C_{\max} - Q_e} + A\exp(-BQ_e). \tag{7}$$

E_0 is the internal electromotive force. $C_{\max}$ is the maximum capacity of the battery. Q_e is the discharge capacity. A, B, K are all fitting parameters, which are obtained from the discharge characteristics of the storm. $A\exp(-BQ_e)$ is the exponential aspect of the initial discharge stage. $KC_{\max}/(C_{\max}-Q_e)$ is the rated characteristic area of the discharge characteristic. Its outer loop control adopts Droop control based on f-P and U-Q. As shown in Fig. 6, the inner loop control adopts the current internal loop control in the $dq0$ rotating coordinate system.

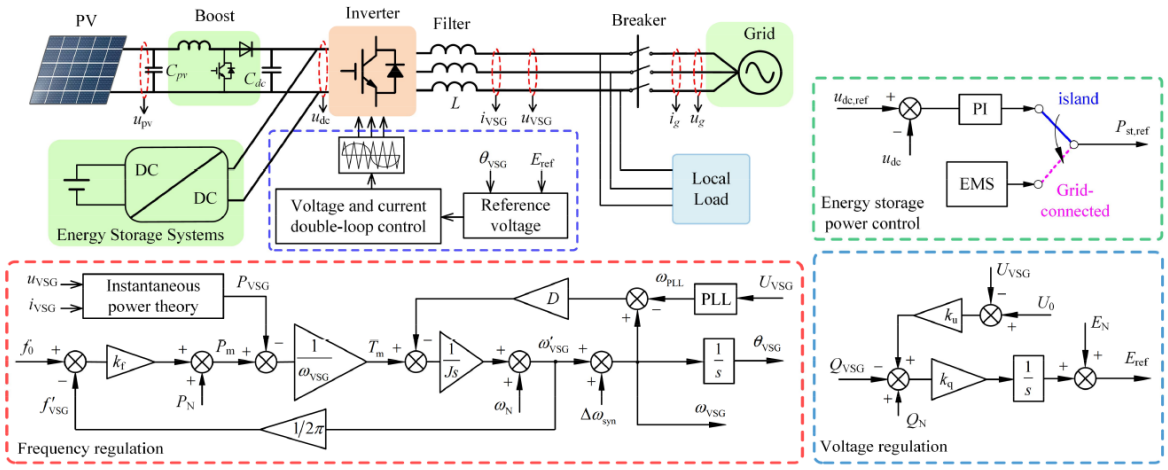

Fig. 6. Typical structure of Droop outer loop controller based on f-P and U-Q

3 Implicit Projection Integration Algorithms

This paper uses the alternating solution method to solve equation (2). At the same time, we use the implicit projection integral algorithm to solve the differential equations. The basic idea of the projection integration algorithm is as follows: First, carry out several steps of small-step integration calculation. The integration step length corresponds to the time constant of the fast dynamic process of the system. Then, according to the small step length calculation result, one step large step length projection integral calculation is performed. The step size corresponds to the time constant of the slow dynamic process of the system. The calculation process of small-

step integration is called internal integration. The method of projection integration with significant steps is called external integration. We determine the constants k and M. The simulation time interval is $t_n - t_{n+k+1+M}$ [7]. The calculation steps of a projection integration step of the implicit projection integration algorithm are as follows:

1) We use the internal integration algorithm to integrate step k. The step size is Δt. In this way, we can get x_{n+k} from x_n. The internal integration algorithm must use an explicit numerical accuracy above the second order.

2) We use the internal integration algorithm to integrate one more step. The step size is still Δt. In this way, x_{n+k+1} can be obtained.

3) We use an external integration algorithm based on the implicit prediction-correction method to obtain $x_{n+k+1+M}$ by integrating a significant step. The step size is $\Delta T = M\,\Delta t$. The implicit prediction-correction method solves the implicit difference form of the active distribution system model. The specific solution steps are as follows.

$$\begin{cases} x_{n+k+1+M} = x_{n+k+1} + \dfrac{1}{2}\Delta T(f(x_{n+k+1}, y_{n+k+1}) + f(x_{n+k+1+M}, y_{n+k+1+M})) \\ g(x_{n+k+1+M}, y_{n+k+1+M}) = 0 \end{cases}. \tag{8}$$

In the formula, ξ is the allowable value of error. If $x^{(1)}_{n+k+1+M}$ satisfies equation (8), the calculation of the external integrator of the implicit projection algorithm is completed. Otherwise, we will replace $x^{(0)}_{n+k+1+M}$ and $y^{(0)}_{n+k+1+M}$ with $x^{(1)}_{n+k+1+M}$ and $y^{(1)}_{n+k+1+M}$ respectively. We repeat steps C and D until the error convergence condition is met.

In the above steps, steps 1) and 2) are the internal integrators of the implicit projection integration algorithm. Step 3) is the external integrator of the implicit projection integration algorithm. The dynamic simulation algorithm flow of the active power distribution system based on implicit projection integral is shown in Fig. 7.

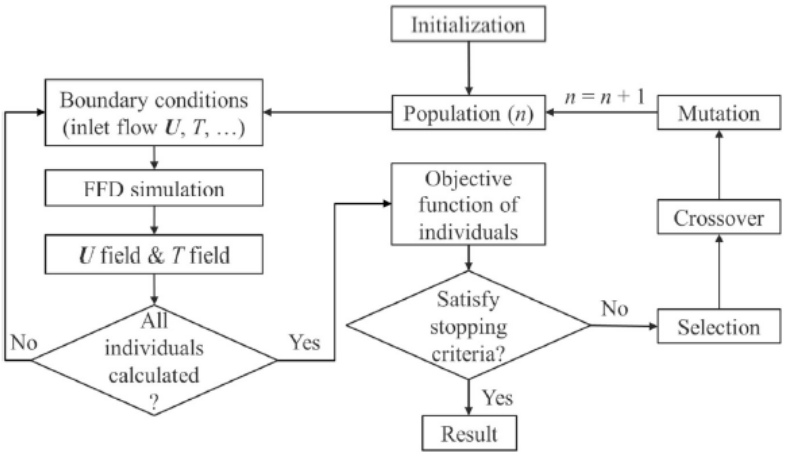

Fig. 7. Dynamic simulation algorithm flow based on implicit projection integral

4 Analysis of Numerical Characteristics of Implicit Projection Algorithm

4.1 Numerical Stability Analysis

This paper uses the internal integration algorithm to take the explicit fourth-order Runge-Kutta method as an example to analyze the numerical stability of the implicit projection integration algorithm. At the same time, we have similar analysis conclusions when using other explicit integration algorithms as internal integration algorithms. The necessary and sufficient condition for the numerical solution of the implicit projection algorithm to

maintain numerical stability is that the error amplification factor satisfies the absolute stability condition. The error amplification factor can be described by equation (9).

$$\sigma(\Delta t\lambda) = \frac{2 + M\Delta t\lambda}{2 - M\Delta t\lambda}\rho^{k+1}(\Delta t\lambda). \tag{9}$$

Where $\rho(\Delta t\lambda)$ is the error amplification factor of an internal integration step of the implicit projection algorithm, namely:

$$\rho(\Delta t\lambda) = 1 + \Delta t\lambda + \frac{(\Delta t\lambda)^2}{2!} + \frac{(\Delta t\lambda)^3}{3!} + \frac{(\Delta t\lambda)^4}{4!}. \tag{10}$$

Fig. 8 shows the numerical stability domain of the explicit fourth-order Runge-Kutta method, the explicit projection algorithm, and the implicit projection algorithm under different parameters in the $\Delta t\lambda$ plane.

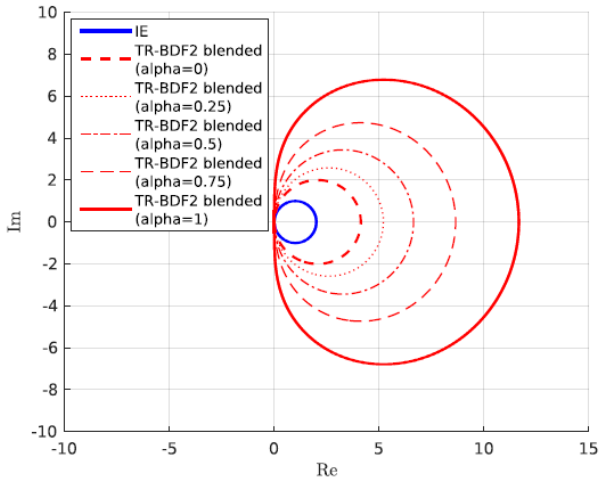

Fig. 8. Explicit and implicit algorithm numerical stability domain comparison

The figure's numerical stability domain of the implicit projection integration algorithm is finite. It is consistent with the shape of the numerical stability region of the fourth-order Runge-Kutta method. When the external integrator step size multiple M is the same, the numerical stability domain of the implicit projection algorithm is more significant than that of the explicit projection algorithm. Therefore, the implicit projection algorithm has better numerical stability than the straightforward projection algorithm [8].

4.2 Numerical Accuracy Analysis

Numerical accuracy indicates the degree to which the numerical solution of each step of the integral operation deviates from its actual value in solving the differential equation of the numerical integration algorithm. The internal integrator of the implicit projection algorithm must adopt an explicit integration algorithm with numerical precision above the second order. Therefore, the process of calculating the internal integrator of the implicit projection algorithm from x_n to obtain x_{n+1} in one step can be described by the Taylor expansion of x_{n+1} at the time t_n. The details are as follows:

$$x_{n+1} = x_n + \sum_{m=1}^{\sigma} \frac{1}{m!}\Delta t^m x_n^{(m)} + O(\Delta t^{\sigma+1}). \tag{11}$$

σ is the order of the internal integrator of the implicit projection algorithm and $\sigma \geq 2$. $O(\Delta t^{\sigma+1})$ is the partial truncation error term for the internal integrator to integrate one step with the step length Δt .

Implicit projection algorithm the external integrator uses an implicit prediction-correction method. The Taylor expansion of $x_{n+k+1+M}$ obtained from x_{n+k+1} using an external integrator is as follows:

$$x_{n+k+1+M} = x_{n+k+1} + (M\Delta t)\dot{x}_{n+k+1} + \frac{1}{2!}(M\Delta t)^2 \ddot{x}_{n+k+1} + O_2((M\Delta t)^3). \tag{12}$$

Where $O_2((M\Delta t)^3)$ is the local truncation error term of the external integrator from t_{n+k+1} to $t_{n+k+1+M}$. The external integrator has a third-order local truncation error and a second-order accuracy. From equations (11) and (12), one projection integration step of the implicit projection algorithm can be obtained. The Taylor expansion from t_n to $t_{n+k+1+M}$ is expressed as follows:

$$x_{n+k+1+M} = x_n + (k+1+M)\Delta t\dot{x}_n + \frac{1}{2!}(k+1+M)^2 \bullet \Delta t\ddot{x}_n + \sum_{m=3}^{\sigma} O_m(\Delta t^m) + O_2((M\Delta t)^3). \tag{13}$$

Where $O_m(\Delta t^m)$ is the high-order term (above the second-order) and the local truncation error term of the internal integrator from t_n to t_{n+k+1} . We compare equation (13) with the actual value of the state variable at time $t_{n+k+1+M}$ to get:

$$\zeta = \sum_{m=3}^{\sigma+1} O_m(\Delta t^m) + O_2((M\Delta t)^3). \tag{14}$$

Where ζ is the residual term of a projection integration step of the implicit projection algorithm and $\sigma \geq 2$. Therefore, the implicit projection algorithm has a third-order truncation error and a second-order accuracy. Its accuracy is determined by the numerical accuracy of the external integrator. The traditional implicit trapezoid method and the implicit projection algorithms are second-order precision algorithms. However, there is still an individual difference in the simulation accuracy between the trapezoidal method and the implicit projection algorithm under different simulation steps. This is caused by the difference in the local truncation error term of the two algorithms.

5 Example Test and Analysis

This paper implements the implicit projection integration algorithm based on the SSDG software platform. The report uses the low-voltage active distribution system example and the IEEE123 node test example to test the algorithm. In this paper, the internal integrator of the implicit projection algorithm takes the explicit fourth-order Runge-Kutta method as an example for simulation testing.

5.1 Example Test One

Overview of Calculation Examples. Example 1 uses a low-voltage active power distribution system example. We test the adaptability of the implicit projection algorithm to dynamic simulation problems with variable structure characteristics. The low-voltage active distribution system example is a radial distribution network test example that conforms to the existing distribution network in China. The network structure is shown in Fig. 9. The voltage level of the calculation example is 400V. The main feeder is connected to the medium voltage bus M1 through a 0.4/10kV transformer [9]. The transformer adopts the DYn11 connection method. The low-voltage side is set to have a reactive power compensation capacitor. The primary feeder node spacing is 50m. We use three-phase symmetrical lines and loads. In the calculation example, a photovoltaic power generation system is connected with maximum power tracking control and a battery energy storage system. The control mode, access capacity, and active power output of each distributed power supply are shown in Table 1.

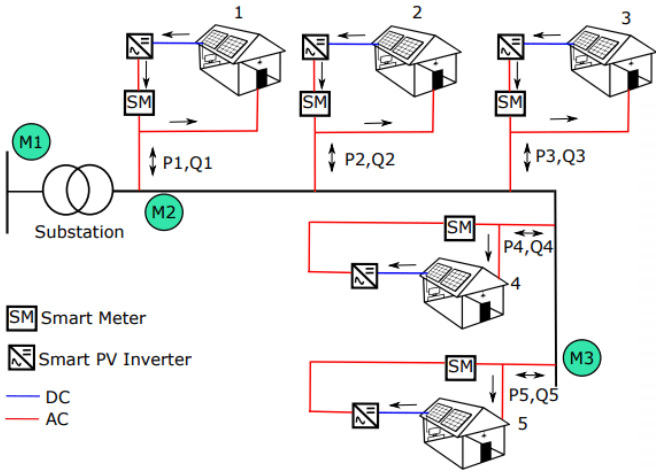

Fig. 9. Example of the low-voltage active power distribution system

Table 1. Distributed power supply control mode, access capacity, and active output

Busbar	Distributed power	Control method	Capacity	Active power
L16	The photovoltaic power generation system	DC voltage and reactive power control Maximum power tracking control	30kWp	20.4kW
L16	Battery energy storage system	Droop control	30kVA	The steady-state output is zero
L17	The photovoltaic power generation system	DC voltage and reactive power control Maximum power tracking control	30kWp	20.4kW
L17	Battery energy storage system	Droop control	30kVA	The steady-state output is zero

Analysis and Verification of Simulation Results Set the Simulation Time to 9s. The simulation step is 0.5ms. At 2.0s, the switch S1 of the low-voltage active power distribution system is turned off. The system switches from grid-connected operation mode to island operation mode. Switch S1 is closed at 4.7s. The system is restored from island operation mode to grid-connected operation mode [10]. The simulation step length of Dig SILENT is the same as the internal integration step length. The simulation results of L17 bus voltage per unit value and No. 2 battery active power output are shown in Fig. 10 [11].

The decrease of the parameter k of the implicit projection algorithm or the increase of M results in a slight deviation between the simulation results and the Power Factory. According to the dynamic simulation results of the L17 bus A-phase voltage, this paper obtains the relative error between the exact projection integration algorithm and the Power Factory simulation results. The purpose is to more intuitively compare the simulation deviation of the explicit projective integration algorithm with Power Factory. It can be seen that the larger the value of parameter k, the smaller the deviation between the results of the exact projection integration algorithm and the commercial software. The larger the value of M, the larger the simulation error of the explicit projective integration algorithm. The maximum relative error is always maintained within 0.3%. The simulation result of the implicit projection algorithm is consistent with the simulation result of the traditional implicit trapezoid method. The result can accurately reflect the dynamic response characteristics of the active power distribution system components after the system structure changes.

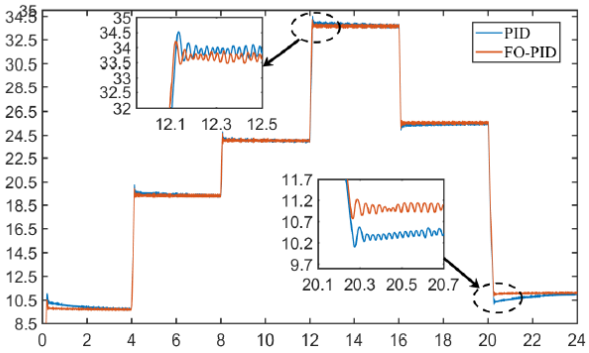

Fig. 10. Simulation results of battery active power output

5.2 Example Test Two

Overview of Calculation Examples. We use a larger-scale IEEE123 node example for testing. The purpose is to test the adaptability and computational efficiency of the implicit projection algorithm for dynamic simulation problems of active power distribution systems with large-scale distributed power sources. The IEEE123 node example is a radial distribution network with a complex structure. The voltage level is 4.16kV. Various types of loads are considered internally [12]. The entire system is connected to the upper-level grid through node 150. The network structure is shown in Fig. 11. The photovoltaic penetration rate reaches 30%.

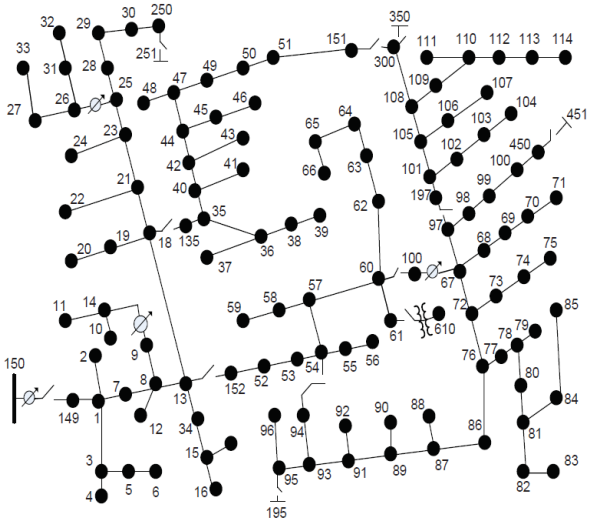

Fig. 11. Example of IEEE123 node

Analysis and Verification of Simulation Results. Set the simulation time to 9s. The initial light intensity of the environment of the calculation example is 1000W/m^2. The light intensity changes to 1025, 1010, and 1000W/m^2 at 2, 4, and 6.5s. We compare the simulation results of the implicit projection algorithm with the results of Dig SILENT and the implicit trapezoid method [13]. The implicit projection algorithm parameter takes $k = 3$, $M = 4$. Take $0.5ms$ as the internal integration step size Δt. The simulation results of photovoltaic active power output and photovoltaic grid-connected bus voltage per unit value at node 61 are shown in Fig. 12.

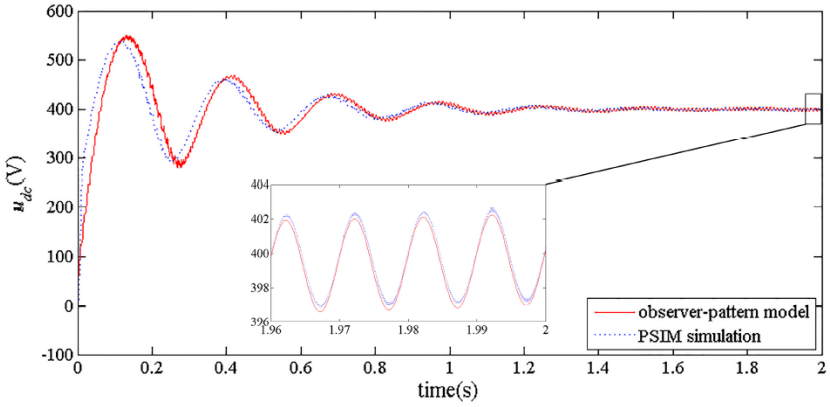

Fig. 12. Simulation results of PV grid-connected bus voltage

The implicit projection algorithm's simulation results are consistent with Dig SILENT's simulation results and the traditional implicit trapezoid method. The implicit projection algorithm has higher simulation accuracy than the implicit trapezoid method, in which the simulation step is taken as the external integration step [14]. In the logarithmic coordinate system, we compare the absolute errors of the implicit projection algorithm and the implicit trapezoidal method simulation results under asynchronous length (Fig. 13). The peak value of the simulation error occurs when the light intensity changes [15]. When Δt_{TR} takes part of the intermediate value of the external integration step length and the internal integration step length, the absolute error of the implicit projection algorithm is slightly lower than that of the implicit trapezoidal method.

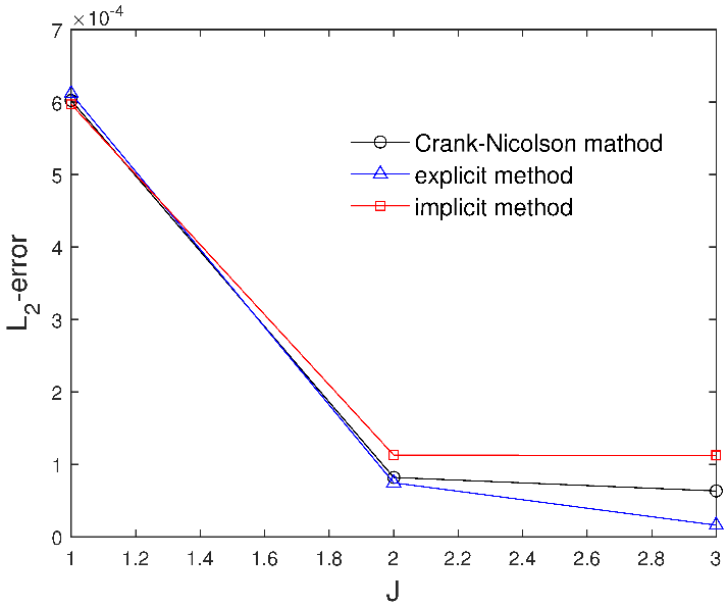

Fig. 13. Numerical accuracy comparison

Simulation Efficiency Test. The implicit projection algorithm has obvious advantages in its numerical stability compared with the explicit projection algorithm. Therefore, we can improve the efficiency of simulation calculation by selecting a more considerable value of M [16]. We use the exact fourth-order Runge-Kutta method with a step length of 0.5ms as the benchmark. Choose different simulation steps and algorithm parameters. Compare the simulation calculation time of implicit projection algorithm, explicit projection algorithm, Dig SILENT, and

traditional implicit trapezoid method under fixed step size.

Compared with the traditional Runge-Kutta method and the commercial software Dig SILENT, the simulation calculation time of the implicit projection algorithm is significantly reduced. As the value of k decreases and the value of M increases, the calculation time of the projection algorithm gradually decreases. When the parameters are the same, the external integrator of the implicit projection algorithm adopts the implicit prediction-correction method [17]. It consumes more computing resources. The computational efficiency of the implicit projection algorithm will be slightly lower than that of the explicit projection algorithm. However, when $k = 3, M = 8$ is taken, the precise projection algorithm is numerically unstable, while the implicit projection algorithm can maintain numerical stability even when M takes 60. At this time, the calculation time of the implicit projection algorithm is much shorter than that of the traditional Runge-Kutta method and Dig SILENT. Compared with the explicit projection algorithm, the calculation efficiency of the implicit projection algorithm has been further improved [18].

The calculation efficiency of the implicit projection algorithm is much higher than that of the trapezoid method when the trapezoidal method simulation step Δt_{TR} takes the internal integration step $\Delta T = 0.5ms$ of the implicit projection algorithm. When Δt_{TR} takes the external integration step size $\Delta T = 20ms$, the calculation efficiency of the implicit projection algorithm is slightly lower than that of the trapezoidal method. The calculation efficiency of the implicit projection algorithm is higher than that of the traditional implicit trapezoid method when Δt_{TR} takes part in the intermediate step length.

6 Conclusion

This paper fully considers the rigid characteristics of dynamic simulation of active power distribution systems. At the same time, this paper proposes a dynamic simulation method of an active power distribution system based on an implicit projection integration algorithm. This method is a 2nd order precision algorithm. Its numerical stability is independent of the external integrator step size multiple. It has similar characteristics to strength. The test results of an example show that the algorithm performance of the implicit projection algorithm is better than that of the traditional implicit trapezoidal method. It has obvious advantages over the exact projection integration algorithm in numerical stability and simulation efficiency. Based on the projection idea, this paper uses the unique numerical stability properties and the combination of different steps and precision algorithms to improve the simulation efficiency. However, this paper does not deal with the dynamic simulation model of the active power distribution system. There is still room for improvement in the computational efficiency of the projection integration algorithm. In the future research process, the author can try to use estimation methods, including subspace (Krylov subspace, mop Chebyshev subspace), to reduce the dimension of the system model to improve the simulation efficiency further.

References

[1] M. Wang, J. Guo, W. Wang, S. Zhang, Smart grid network resource scheduling algorithm based on network calculus, Integrated Ferroelectrics 199(1)(2019) 1-11.

[2] V. Pliuhin, V. Teterev, A. Lapko, Smart Grid technologies as a concept of innovative energy development: initial proposals for the development of Ukraine, Lighting Engineering & Power Engineering 60(2)(2021) 47-65.

[3] G. Tsaousoglou, K. Steriotis, N. Efthymiopoulos, P. Makris, E. Varvarigos, Truthful, practical and privacy-aware demand response in the smart grid via a distributed and optimal mechanism, IEEE Transactions on Smart Grid 11(4)(2020) 3119-3130.

[4] J. Singh, R. Tiwari, Real power loss minimisation of smart grid with electric vehicles using distribution feeder reconfiguration, IET Generation, Transmission & Distribution 13(18)(2019) 4249-4261.

[5] T. Zhen, T. Elgindy, S.M. Alam, B.M. Hodge, C.D. Laird, Optimal placement of data concentrators for expansion of the smart grid communications network, IET Smart Grid 2(4)(2019) 537-548.

[6] O.M. Butt, M. Zulqarnain, T.M. Butt, Recent advancement in smart grid technology: Future prospects in the electrical power network, Ain Shams Engineering Journal 12(1)(2021) 687-695.

[7] X. Luo, K. Xue, J. Xu, Q. Sun, Y. Zhang, Blockchain Based Secure Data Aggregation and Distributed Power Dispatching for Microgrids, IEEE Transactions on Smart Grid 12(6)(2021) 5268-5279.

[8] P. Lin, P. Wang, C. Jin, J. Xiao, X. Li, F. Guo, C. Zhang, A distributed power management strategy for multi-paralleled bidirectional interlinking converters in hybrid AC/DC microgrids, IEEE Transactions on Smart Grid 10(5)(2019) 5696-

5711.
[9] N.I. Nimalsiri, C.P. Mediwaththe, E.L. Ratnam, M. Shaw, D.B. Smith, S.K. Halgamuge, A survey of algorithms for distributed charging control of electric vehicles in smart grid, IEEE Transactions on Intelligent Transportation Systems 21(11)(2020) 4497-4515.
[10] M. Ghiasi, N. Ghadimi, E. Ahmadinia, An analytical methodology for reliability assessment and failure analysis in distributed power system, SN Applied Sciences 1(1)(2019) 1-9.
[11] D. Du, X. Li, W. Li, R. Chen, M. Fei, L. Wu, ADMM-based distributed state estimation of smart grid under data deception and denial of service attacks, IEEE Transactions on Systems, Man, and Cybernetics: Systems 49(8)(2019) 1698-1711.
[12] H. Tu, Y. Du, H. Yu, A. Dubey, S. Lukic, G. Karsai, Resilient information architecture platform for the smart grid: A novel open-source platform for microgrid control, IEEE Transactions on Industrial Electronics 67(11)(2020) 9393-9404.
[13] A. Kumari, S. Tanwar, N. Tyagi, N. Kumar, M.S. Obaidat, J.J. Rodrigues, Fog computing for smart grid systems in the 5G environment: Challenges and solutions, IEEE Wireless Communications 26(3)(2019) 47-53.
[14] C.W. Yang, V. Dubinin, V. Vyatkin, Automatic generation of control flow from requirements for distributed smart grid automation control, IEEE Transactions on Industrial Informatics 16(1)(2020) 403-413.
[15] F. Li, J. Qin, W.X. Zheng, Distributed Q -Learning-Based Online Optimization Algorithm for Unit Commitment and Dispatch in Smart Grid, IEEE transactions on cybernetics 50(9)(2020) 4146-4156.
[16] A. Abdukhakimov, S. Bhardwaj, G. Gashema, D.S. Kim, Reliability analysis in smart grid networks considering distributed energy resources and storage devices, International Journal of Electrical and Electronic Engineering & Telecommunications 8(5)(2019) 233-237.
[17] S.K. Rathor, D Saxena, Energy management system for smart grid: An overview and key issues, International Journal of Energy Research 44(6)(2020) 4067-4109.
[18] U. Shahzad, Smart grid and electric vehicle: overview and case study, Journal of Electrical Engineering, Electronics, Control and Computer Science 8(27)(2022) 1-6.